Propulsion of a foil undergoing a flapping undulatory motion from the impulse theory in the linear potential limit

J. ALAMINOS-QUESADA AND R. FERNANDEZ-FERIA

Fluid Mechanics, Universidad de Málaga, Andalucía Tech, Dr Ortiz Ramos s/n, 29071 Málaga, Spain

(Received 19 October 2019)

We derive general analytical expressions for the aerodynamic force and moment on a flapping flexible foil undergoing a prescribed undulatory motion in a two-dimensional, incompressible and linearized potential flow from the vortical impulse theory. We consider a fairly broad class of foil motion, characterized by nine nondimensional parameters in addition to the reduced frequency. Quite simple analytical expressions are obtained in the particular case when just a chordwise flexure mode is superimposed to a pitching or heaving motion of the foil, for which the optimal conditions generating a maximum thrust force and a maximum propulsion efficiency are mapped in terms of the reduced frequency and the relative amplitude and phase shift of the deflection of the foil. These results are discussed in relation to the optimal conditions for a pitching or heaving rigid foil. The present theoretical results are compared with available numerical data for some particular undulatory motions of the flexible foil, with good agreement for small amplitudes of the oscillations and sufficiently high Reynolds number.

1. Introduction

Unsteady aerodynamics of flapping foils is an area of active research in part due to the recent interest in the development of small unmanned aerial and aquatic vehicles, bioinspired by flying and swimming animals. It is well known that flexible structures can enhance the propulsive performance of flapping flight and swimming (Wu 1971*b*; Katz & Weihs 1978; Prempraneerach *et al.* 2003; Pederzani & Haj-Hariri 2006; Heathcote & Gursul 2007; Zhu 2007; Alben 2008; Kang *et al.* 2011; Ramananarivo *et al.* 2011; Dewey *et al.* 2013; Moore 2014; Huera-Huarte 2018), which is supported by the fact that most flying and swimming animals take advantage of the flexibility of their flapping appendages to increase lift, thrust, and/or propulsive efficiency depending on the particular circumstances of their locomotion (Lighthill 1975; Wu *et al.* 1975; Vogel 1994; Shyy *et al.* 2013). Although the rigid wing aerodynamics has been explored in more detail than the flexible wing aerodynamics (see, e.g., Platzer *et al.* 2008), numerous experimental and numerical studies have appeared recently on flexible flapping foils (see, e.g., Shyy *et al.* 2010; Wu 2011; Wang & Zhang 2016).

Avoiding the interesting and more complex issue of the fluid-structure interaction (Michelin & Llewellyn Smith 2009; Dewey *et al.* 2013; Moore 2014; Paraz *et al.* 2016; Tzezana & Breuer 2019), one of the most interesting problems is the characterization of the aerodynamic performance for prescribed kinematics of the flexible foil, which allows to search the foil motion that maximizes thrust and/or propulsive efficiency. As in the case of a rigid flapping foil, despite the great advances in numerical simulations and experimental studies, linear unsteady potential theory still constitutes a powerful analytical tool to understand, and to estimate, the aerodynamic performance of flexible flapping foils. The theory was originally developed for two-dimensional (2D) foils undergoing an arbitrary harmonic motion by Wu and Lighthill (Wu 1961; Lighthill 1970; Wu 1971*b*,*a*), containing the pitching and heaving motion of a rigid foil as a particular case, which was previously studied by Theodorsen (1935) for the lift and moment, and by Garrick (1936) for the thrust and propulsion efficiency. Using this classical linear potential theory, the optimisation problem of the propulsive performance has been addressed for the pitching and heaving oscillating motion of a rigid foil, and for the more complex undulatory motion of a flexible foil by several authors (Lighthill 1970; Wu 1971*a*; Alben 2008; Eloy & Schouveiler 2011; Eloy 2013; Moore 2015; Floryan & Rowley 2018).

Of particular relevance to address the problem of the unsteady aerodynamics of slender bodies at high Reynolds number is the vortical impulse theory in the limit of linearized inviscid flows,

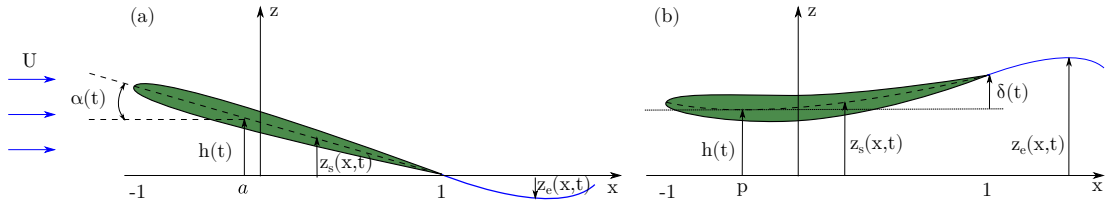

Figure 1: Schematic of the oscillating foil for heaving and pitching rigid motion (a) and for heaving and flexural motion (b), both in absence of undulatory motion (i.e., for $\mathsf{b} = 0$). See equations (2.1)-(2.4) for the meaning of the different nondimensional quantities.

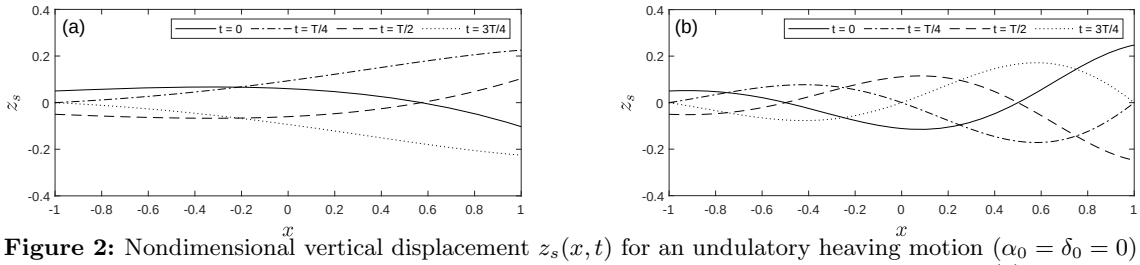

Figure 2: Nondimensional vertical displacement $z_s(x,t)$ for an undulatory heaving motion ($\alpha_0 = \delta_0 = 0$) at different instants of the period's oscillation T for $h_0 = 0.05$, $b_1 = 0.8$, with $b_2 = 1$ in (a), and with $b_2 = \pi$ in (b) [see equations (2.1)-(2.4) for the nondimensional notation].

because of the insight that it provides on the effect of unsteadiness on the physics behind the aerodynamic force and moment. This approach was first utilised by von Kármán & Sears (1938) to obtain the lift force and moment on a rigid foil undergoing an arbitrary motion, and recently extended to include the thrust force and the propulsive efficiency of a pitching and heaving rigid foil (Fernandez-Feria 2016). This last formulation corrects, for moderate and high reduced frequencies, Grarrick's (1936) result for the thrust force produced by a rigid oscillating foil, which was assumed to be primarily generated by the leading-edge suction. Thus, the impulse formulation substantially modifies the prediction of the kinematic conditions that optimise the propulsion efficiency of a heaving and pitching rigid foil (Fernandez-Feria 2017), especially for high reduced frequencies. In the present paper we generalize this vortical impulse theory to a flexible foil undergoing a quite general undulatory motion, of interest for the locomotion of a great variety of swimming and flying animals, to obtain analytical expressions for the lift, thrust, moment, and propulsive efficiency. These general analytical expressions, which contain as a limit those previously obtained for a pitching and heaving rigid foil, are validated against available numerical results for some particular undulatory kinematics of the flexible foil. The analytical expressions are quite useful to characterize the foil's kinematics that generates an optimal propulsion. In particular, we include results for the case when a chordwise flexure mode is added to the motion of a heaving and of a pitching foil, characterizing the kinematics parameters that optimise both the thrust force and the propulsion efficiency in relation to the rigid heaving and the rigid pitching counterparts, respectively.

2. Formulation of the problem. Kinematics

We consider the two-dimensional, incompressible and nearly inviscid flow over a flexible thin foil of chord length c that moves with constant speed U along the negative x-axis. Superimposed to heaving and pitching motions [see Fig. 1(a)], the plate undergoes an undulating motion with a given wavelength (defined below), and a quadratic flexure (or deflection) motion of trailing edge amplitude δ_m [see Fig. 1(b)]. All the amplitudes are small compared with the chord c, so that the airfoil, and every point of the trail of vortices that it leaves behind, may be considered to be on the horizontal plane $z = 0$ in first approximation.

We use nondimensional variables scaled with the half-chord length $c/2$ and the velocity U, so that the plate extends from $x = -1$ to $x = 1$ in a reference frame translating with it at speed U along the x-axis (see Fig. 1), and the nondimensional time t is scaled with $c/(2U)$. In this reference frame, the vertical motion of the foil, given by the vertical displacement of its mean-chamber line z_s, can be written as

$$z_s(x,t) = h(x,t) - (x-a)\alpha(x,t) + (x-p)^2\delta(x,t), \quad -1 \leqslant x \leqslant 1, \tag{2.1}$$

with

$$h(x,t) = \Re\left[h_0 e^{ikt+\mathsf{b}(x+1)}\right], \quad \alpha(x,t) = \Re\left[\alpha_0 e^{ikt+\mathsf{b}(x+1)}\right], \quad \delta(x,t) = \Re\left[\delta_0 e^{ikt+\mathsf{b}(x+1)}\right], \tag{2.2}$$

$$\mathsf{b} = b_1 - ib_2, \quad k = \frac{\omega c}{2U}. \tag{2.3}$$

In these expressions $\Re$ means real part and k is the reduced frequency associated to the frequency ω of the harmonic motion, with nondimensional period $T = 2\pi/k$, which consists of a heaving displacement $h(x,t)$, a pitching rotation $\alpha(x,t)$ pivoting at $x = a$, and a quadratic deflection motion $\delta(x,t)$ pivoting at $x = p$. Superimposed to each of these three displacements, we have included an undulatory motion of the foil with nondimensional wave number b_2 whose amplitude grows exponentially to the trailing edge with a nondimensional factor b_1, both quantities grouped together in the complex number b. This form, motivated by the analysis of the carangiform fish dynamics by Lighthill (1970), produces a traveling wave of growing amplitude that propagates from the leading edge to the trailing edge with nondimensional phase speed k/b_2. Figure 2 shows some examples when the pitching and flexure motions are absent.

The amplitudes h_0, α_0 and δ_0 are, in general, complex constants satisfying $|h_0| \ll 1$, $|\alpha_0| \ll 1$ and $|\delta_0| \ll 1$. For simplicity we select h_0 real and

$$\alpha_0 = a_0 e^{i\phi}, \quad \delta_0 = \frac{\delta_m}{(1-p)^2} e^{i\psi}, \tag{2.4}$$

with ϕ the phase shift between the heaving and pitching motions of the foil, ψ the phase shift between the heaving and deflection motions, a_0 the maximum pitch amplitude of the plate, and δ_m the maximum amplitude of the flexure component of the motion at the trailing edge ($x = 1$). In what follows we shall work with the complex expressions knowing that we have to take the real part of the results. Equations (2.1)-(2.4) describe a fairly broad class of the flapping undulatory motion of a flexible or complian foil, with nine nondimensional kinematic parameters (plus the reduced frequency), for which we shall derive analytical expressions for the force and moment using the impulse theory in the linear potential limit. General undulatory kinematics, with infinitely many wave numbers, have been considered numerically by several authors both in the present small-amplitude inviscid limit (e.g., Alben 2008; Moore 2017; Tzezana & Breuer 2019) or using direct numerical simulation of the Navier-Stokes equations (e.g., Hoover *et al.* 2018).

To facilitate the computations, the vertical displacement of the foil will be written as

$$z_s(x,t) = \left[\mathcal{F}(t) + \mathcal{E}(t)x + \mathcal{D}(t)x^2\right] e^{\mathsf{b}x}, \quad -1 \leqslant x \leqslant 1, \tag{2.5}$$

where $\mathcal{F}(t), \mathcal{E}(t)$, and $\mathcal{D}(t)$ are given by

$$\mathcal{F}(t) \equiv \left(h_0 + a\alpha_0 + p^2\delta_0\right) e^{ikt+\mathsf{b}} \equiv \mathcal{F}_0 e^{ikt+\mathsf{b}}, \tag{2.6}$$

$$\mathcal{E}(t) \equiv -\left(\alpha_0 + 2p\delta_0\right) e^{ikt+\mathsf{b}} \equiv \mathcal{E}_0 e^{ikt+\mathsf{b}}, \tag{2.7}$$

$$\mathcal{D}(t) \equiv \delta_0 e^{ikt+\mathsf{b}}. \tag{2.8}$$

The corresponding nondimensional vertical velocity of the foil's mean-chamber line can be written as

$$v_0(x,t) = \frac{\partial z_s}{\partial t} + \frac{\partial z_s}{\partial x} = \left[\mathcal{A}(t) + \mathcal{B}(t)x + \mathcal{C}(t)x^2\right] e^{\mathsf{b}x}, \quad -1 \leqslant x \leqslant 1, \tag{2.9}$$

where $\mathcal{A}(t), \mathcal{B}(t)$, and $\mathcal{C}(t)$ are given by

$$\mathcal{A}(t) \equiv \left\{(ik+\mathsf{b})\mathcal{F}_0 + \mathcal{E}_0\right\} e^{ikt+\mathsf{b}} \equiv \mathcal{A}_0 e^{ikt+\mathsf{b}}, \tag{2.10}$$

$$\mathcal{B}(t) \equiv \left\{(ik+\mathsf{b})\mathcal{E}_0 + 2\delta_0\right\} e^{ikt+\mathsf{b}} \equiv \mathcal{B}_0 e^{ikt+\mathsf{b}}, \tag{2.11}$$

$$\mathcal{C}(t) \equiv (ik+\mathsf{b})\,\delta_0 e^{ikt+\mathsf{b}} \equiv \mathcal{C}_0 e^{ikt+\mathsf{b}}. \tag{2.12}$$

3. General expressions for the lift, thrust, moment and input power

The vortical impulse theory for an incompressible and unbounded flow (Wu 1981) is used to obtain the force and moment on the airfoil. Neglecting the volume (section) of the airfoil, the total force $\mathbf{F}$ can be written as

$$\mathbf{F} \equiv D\mathbf{e}_x + L\mathbf{e}_z = -\rho\frac{d\mathbf{I}}{dt}, \tag{3.1}$$

where the $x-$component D is the drag (or minus the thrust), the $z-$component L is the lift, ρ the fluid density, and the vortical impulse (or vorticity moment) $\mathbf{I}$ is defined as

$$\mathbf{I} = \int_{\mathcal{V}} \mathbf{x} \wedge \boldsymbol{\omega} d\mathcal{V}, \tag{3.2}$$

where $\boldsymbol{\omega} = \nabla \wedge \mathbf{v}$ is the vorticity field and $\mathcal{V}$ is the entire volume (plane surface in this case) occupied by the fluid plus the airfoil. In writing (3.1) it is assumed that $\mathcal{V}$ is unbounded and that the flow is potential far from the airfoil. In fact, we shall assume that the vorticity, which is directed along the normal $\mathbf{e}_y$ to the plane of the fluid motion, is concentrated on the airfoil surface and in its trailing wake, both of them considered as planar (bound and free, respectively) vortex sheets. Thus,

$$\mathbf{I} \simeq \int_{-1}^{1} \left(-z_s \varpi_s \mathbf{e}_x + x \varpi_s \mathbf{e}_z\right) dx + \int_{1}^{\infty} \left(-z_e \varpi_e \mathbf{e}_x + x \varpi_e \mathbf{e}_z\right) dx, \tag{3.3}$$

where $\varpi_s(x,t)$ is the vorticity density distribution on the airfoil, $\varpi_e(x,t)$ is the vorticity density distribution in the trailing wake, and $z_e(x,t)$ is the vertical position of each point in this vortex wake (see Fig. 1). We consider the large-time behavior in which the vortex wake sheet extends many chord lengths downstream of the airfoil, so that, in first approximation, $1 \leqslant x \leqslant \infty$ for both $\varpi_e(x,t)$ and $z_e(x,t)$, with $|z_e| \ll 1$ in the present linear approximation. Consequently, under the assumptions made, the total drag and lift force components can be written as

$$D = \rho \frac{d}{dt}\left[\int_{-1}^{1} z_s \varpi_s dx + \int_{1}^{\infty} z_e \varpi_e dx\right], \tag{3.4}$$

$$L = -\rho \frac{d}{dt}\left[\int_{-1}^{1} x \varpi_s dx + \int_{1}^{\infty} x \varpi_e dx\right], \tag{3.5}$$

Similarly, the vortical impulse theory also provides the total moment on the airfoil (Wu 1981)

$$\mathbf{M} = -M \mathbf{e}_y = -\rho \frac{d\mathbf{A}}{dt}, \tag{3.6}$$

where

$$\mathbf{A} = -\frac{1}{2} \int_{\mathcal{V}} |\mathbf{x} - a\mathbf{e}_x|^2 d\mathcal{V}, \tag{3.7}$$

is the angular impulse in relation to the pitching axis $x = a$ moving with speed U along the x-axis (note that the distance Ut is also scaled with $c/2$). Thus, on using the same approximations made in (3.3),

$$M \simeq \frac{1}{2}\rho \frac{d}{dt}\left[\int_{-1}^{1} (x-a)^2 \varpi_s dx + \int_{1}^{\infty} (x-a)^2 \varpi_e dx\right]. \tag{3.8}$$

Finally, the input power is given by

$$P = \int_{-1}^{1} \Delta p \frac{\partial z_s}{\partial t} dx, \tag{3.9}$$

where $\Delta p(x,t) \equiv p_+(x,t) - p_-(x,t)$ is the local pressure difference between both sides of the foil, with subscripts $+$ and $-$ denoting its upper and lower surfaces, respectively. Δp can be obtained from the unsteady Bernoulli equation on the foil surface as

$$\Delta p = -\rho \frac{\partial}{\partial t}(\Delta \Phi) - \frac{1}{2}\rho (u_+^2 - u_-^2), \tag{3.10}$$

where Φ is the velocity potential and u the tangential velocity component. Taking into account that

$$\Delta \Phi = \int_{-1}^{x} (u_+ - u_-) dx, \quad \varpi_s = u_+ - u_-, \quad U = \frac{1}{2}(u_+ + u_-), \tag{3.11}$$

and substituting into equation (3.9), the input power can be written in terms of the vorticity distribution as

$$P = -\rho U \int_{-1}^{1} \varpi_s \frac{\partial z_s}{\partial t} dx - \rho \int_{-1}^{1} \left(\int_{-1}^{x} \frac{\partial \varpi_s}{\partial t} d\xi\right) \frac{\partial z_s}{\partial t} dx, \tag{3.12}$$

which, after integrating by parts the double integral, can be more conveniently written as

$$P = -\rho U \int_{-1}^{1} \varpi_s \frac{\partial z_s}{\partial t} dx - \rho \int_{-1}^{1} \left(\int_{x}^{1} \frac{\partial z_s}{\partial t} d\xi \right) \frac{\partial \varpi_s}{\partial t} dx. \tag{3.13}$$

3.1. *Vorticity distribution*

Following von Kármán & Sears (1938), who used the above linearized version of the impulse theory in the inviscid limit for the lift and for the moment on a rigid airfoil (but not for the thrust) much earlier than Wu's (1981) general impulse formulation was derived, and invoking the linearity of the problem, we separate the different contributions to the vorticity on the airfoil as

$$\varpi_s(x,t) = \varpi_0(x,t) + \varpi_{se}(x,t), \tag{3.14}$$

where the first term ϖ_0, with associated circulation

$$\Gamma_0(t) = \int_{-1}^{1} \varpi_0(x,t) dx, \tag{3.15}$$

is the quasi-steady contribution, i.e., that for an airfoil without considering the effect of its unsteady wake, such that the corresponding lift would be $\rho U \Gamma_0$. The last term in (3.14), ϖ_{se}, is the contribution to ϖ_s induced by its wake vortex-sheet, of strength ϖ_e [remember from (3.3) that subscript s stands for the surface of the foil and e for the trailing wake].

Kelvin's total-circulation conservation theorem requires that

$$\Gamma_0 + \Gamma_{se} + \int_{1}^{\infty} \varpi_e(\xi,t) d\xi = 0, \tag{3.16}$$

with

$$\Gamma_{se}(t) = \int_{-1}^{1} \varpi_{se}(x,t) dx. \tag{3.17}$$

To obtain ϖ_0 and ϖ_{se} one has to apply the boundary condition of the vertical velocity (2.9) at $z = 0$, for $-1 \leqslant x \leqslant 1$, which is induced by the whole vorticity distribution. From the linearity of the problem, one may separate the two different sources (see, e.g., Newman 1977; Fernandez-Feria & Alaminos-Quesada 2018) to obtain the following two integral equations for ϖ_0 and ϖ_{se}:

$$v_0(x,t) = \frac{1}{2\pi} \fint_{-1}^{1} \frac{\varpi_0(\xi,t)}{\xi - x} d\xi, \tag{3.18}$$

$$-\frac{1}{2\pi} \int_{1}^{\infty} \frac{\varpi_e(\xi,t)}{\xi - x} d\xi = \frac{1}{2\pi} \fint_{-1}^{1} \frac{\varpi_{se}(\xi,t)}{\xi - x} d\xi, \tag{3.19}$$

where $\fint$ denotes Cauchy's principal value of the integral (e.g., Butkov 1968, chapter 2) and v_0 is given by (2.9). The solution of these singular, linear integral equations of the first kind with constant integration limits are given by (Polyanin & Manzhirov 1998)

$$\varpi_0(x,t) = \frac{1}{\sqrt{1-x^2}} \left\{ \frac{\Gamma_0(t)}{\pi} - \frac{2}{\pi} \fint_{-1}^{1} \frac{\sqrt{1-\xi^2}}{\xi - x} \left[\mathcal{A}(t) + \mathcal{B}(t)\xi + \mathcal{C}(t)\xi^2 \right] e^{\mathsf{b}\xi} d\xi \right\}, \tag{3.20}$$

$$\varpi_{se}(x,t) = \frac{1}{\pi} \sqrt{\frac{1-x}{1+x}} \int_{1}^{\infty} \sqrt{\frac{\xi+1}{\xi-1}} \frac{\varpi_e(\xi,t)}{\xi - x} d\xi, \tag{3.21}$$

where the regularity of ϖ_s at its corresponding trailing edge $x = 1$, or Kutta condition, has been applied. In addition, substituting into equations (3.15) and (3.17) one obtains

$$\Gamma_0(t) = -2\pi \left\{ \mathcal{A}(t) I_0(\mathsf{b}) + \left[\mathcal{A}(t) + \left(1 + \frac{1}{\mathsf{b}} \right) (\mathcal{B}(t) + \mathcal{C}(t)) \right] I_1(\mathsf{b}) + \left[\mathcal{B}(t) + \mathcal{C}(t) \left(1 - \frac{1}{\mathsf{b}} \right) \right] I_2(\mathsf{b}) \right\}, \tag{3.22}$$

$$\Gamma_{se}(t) = \int_{1}^{\infty} \left(\sqrt{\frac{\xi+1}{\xi-1}} - 1 \right) \varpi_e(\xi,t) d\xi, \tag{3.23}$$

where $I_n(\mathsf{b})$, $n = 0, 1, 2$, is the modified Bessel function of the first kind and order n (Olver & Maximon 2010) applied to the complex number b.

Finally, from Kelvin's theorem (3.16), and considering that the vorticity in the wake is convected downstream with velocity U, so it remains constant in a reference frame moving with the fluid,

$$\varpi_e(\xi, t) = \varpi_e(X), \quad z_e(\xi, t) = z_e(X), \quad X = \xi - Ut, \tag{3.24}$$

the wake vorticity distribution ϖ_e is given by the well-known solution in terms of Γ_0 (Theodorsen 1935; von Kármán & Sears 1938)

$$\varpi_e(\xi, t) = \frac{2\Gamma_0(t)}{\pi} \frac{e^{-ik\xi}}{iH_0^{(2)}(k) + H_1^{(2)}(k)}, \tag{3.25}$$

where $H_n^{(2)}(z) = J_n(z) - iY_n(z)$, $n = 0, 1$, is the Hankel function of the second kind and order n, related to the Bessel functions of the first and second kind $J_n(z)$ and $Y_n(z)$ (Olver & Maximon 2010).

3.2. *Lift, thrust, moment and input power*

Taking into account (3.24), the temporal derivatives of ϖ_e and z_e in the general expressions for D, L and M can be easily computed using Leibniz' rule. For the lift one obtains, in nondimensional form,

$$C_L = \frac{L}{\frac{1}{2}\rho U^2 c} = C_{L0} + C_{L1} + C_{L2}, \tag{3.26}$$

where

$$C_{L0} = \Gamma_0, \quad C_{L1} = -\frac{d}{dt}\int_{-1}^{1} x\varpi_0(x, t)dx, \quad C_{L2} = \int_1^\infty \frac{\varpi_e(\xi, t)}{\sqrt{\xi^2 - 1}}d\xi, \tag{3.27}$$

are the quasi-steady lift, the apparent-mass lift and the lift induced by its own unsteady wake. Solving the integrals,

$$C_L = -2\pi\frac{ik}{\mathsf{b}}\left[\left(\mathcal{A} + \mathcal{C}\right)I_1(\mathsf{b}) + \left(\mathcal{B} - \frac{3}{\mathsf{b}}\mathcal{C}\right)I_2(\mathsf{b})\right] + \Gamma_0 C(k), \tag{3.28}$$

where $C(k)$ is the Theodorsen function given by

$$C(k) = \frac{H_1^{(2)}(k)}{iH_0^{(2)}(k) + H_1^{(2)}(k)} = F(k) + iG(k). \tag{3.29}$$

To compute D from (3.4) one assumes that the vertical displacement of the wake coincides with the trailing edge location at the time $t' = t + (1 - \xi)/U$ when it was shed from the airfoil, $z_s(1, t')$; i.e.,

$$z_e(X) = h\left(\frac{1 - X}{U}\right) - (1 - a)\alpha\left(\frac{1 - X}{U}\right) + (1 - p)^2\delta\left(\frac{1 - X}{U}\right). \tag{3.30}$$

Thus,

$$\frac{d}{dt}\int_1^\infty z_e\varpi_e d\xi = z_s(1, t)\varpi_e(1, t). \tag{3.31}$$

Therefore, the thrust, or minus the drag (3.4), in nondimensional form can be written as

$$C_T = \frac{T}{\frac{1}{2}\rho U^2 c} = -\frac{d}{dt}\Big\{\Re[\Gamma_0] \times \Re[\mathcal{Q}(\mathcal{F}, \mathcal{E}, \mathcal{D})] + \Re[\mathcal{A}] \times \Re[\Omega_0(\mathcal{F}, \mathcal{E}, \mathcal{D})] + \Re[\mathcal{B}] \times \Re[\Omega_1(\mathcal{F}, \mathcal{E}, \mathcal{D})] + \Re[\mathcal{C}] \times \Re[\Omega_2(\mathcal{F}, \mathcal{E}, \mathcal{D})]\Big\} - \frac{2k}{\pi}\Re[\Gamma_0 C_1(k)] \times \Re\left\{\left[\mathcal{F} + \mathcal{E} + \mathcal{D}\right]e^{\mathsf{b}}\right\}, \tag{3.32}$$

where the functions $\mathcal{Q}$, Ω_n and $C_1(k)$ are defined as

$$\mathcal{Q}(\tilde{a}, \tilde{b}, \tilde{c}) = \tilde{a}\left(I_0(\mathsf{b}) + \mathcal{J}_0\right) + \tilde{b}\left(I_1(\mathsf{b}) + \mathcal{J}_1\right) + \tilde{c}\left(\frac{I_1(\mathsf{b})}{\mathsf{b}} + I_2(\mathsf{b}) + \mathcal{J}_2\right), \tag{3.33}$$

$$\Omega_n(\tilde{a}, \tilde{b}, \tilde{c}) = \tilde{a}\mathcal{I}_{0,n} + \tilde{b}\mathcal{I}_{1,n} + \tilde{c}\mathcal{I}_{2,n}, \quad n = 0, 1, 2, \tag{3.34}$$

$$C_1(k) = \frac{\frac{1}{k}e^{-ik}}{iH_0^{(2)}(k) + H_1^{(2)}(k)} = F_1(k) + iG_1(k). \tag{3.35}$$

and the functions $\mathcal{J}_n$ and $\mathcal{I}_{n,m}$ are given by

$$\mathcal{J}_n(\mathsf{b},k) \equiv \frac{2/\pi^2}{iH_0^{(2)}(k) + H_1^{(2)}(k)} \int_{-1}^{1} x^n e^{\mathsf{b}x} \sqrt{\frac{1-x}{1+x}} \left(\int_1^{\infty} \sqrt{\frac{\xi+1}{\xi-1}} \frac{e^{-ik\xi}}{\xi - x} d\xi \right) dx = \mathcal{J}_n^R + i\mathcal{J}_n^I, \tag{3.36}$$

$$\mathcal{I}_{n,m}(\mathsf{b}) \equiv -\frac{2}{\pi} \int_{-1}^{1} \frac{x^n e^{\mathsf{b}x}}{\sqrt{1-x^2}} \left(\int_{-1}^{1} \frac{\sqrt{1-\xi^2}}{\xi - x} \xi^m e^{\mathsf{b}\xi} d\xi \right) dx = \mathcal{I}_{n,m}^R + i\mathcal{I}_{n,m}^I, \quad n,m = 0,1,2, \tag{3.37}$$

where, in general, these last integrals have to be solved numerically. It should be noted that $\mathcal{I}_{1,1} = \mathcal{I}_{2,2} = 0$ and $\mathcal{I}_{0,0} = \mathcal{I}_{2,0}$. In addition, when the growth factor of the undulatory motion vanishes ($b_1 = 0$),

$$\mathcal{I}_{0,0}^R = \mathcal{I}_{0,1}^I = {}^R_{0,2} = 0, \quad \mathcal{I}_{1,0}^I = \mathcal{I}_{1,1} = \mathcal{I}_{1,2}^I = 0, \quad \mathcal{I}_{2,0}^R = \mathcal{I}_{2,1}^I = \mathcal{I}_{2,2} = 0, \tag{3.38}$$

where the superscripts R and I denote real and imaginary part, respectively. As discussed in Fernandez-Feria (2016) for a rigid foil, this impulse formulation includes the leading edge suction force together with all the other contributions to the thrust force coming from the vorticity distributions on the airfoil and the vortex wake.

The moment (3.8) can be written, in nondimensional form, as

$$C_M = \frac{M}{\frac{1}{2}\rho U^2 c^2} = C_{M0} + C_{M1} + C_{M2} + \frac{a}{2}C_L, \tag{3.39}$$

where

$$C_{M0} = -\frac{1}{2}\int_{-1}^{1} x\varpi_0(x,t)dx, \quad C_{M1} = \frac{1}{4}\frac{d}{dt}\int_{-1}^{1}\left(x^2 - \frac{1}{2}\right)\varpi_0(x,t)dx, \quad C_{M2} = \frac{C_{L2}}{4}. \tag{3.40}$$

Solving the integrals,

$$\begin{aligned} C_M = {} & \frac{\Gamma_0}{2}\left[C(k)\left(\frac{1}{2}+a\right) - 1\right] - \frac{\pi}{\mathsf{b}}(ika+1)\left[\left(\mathcal{A}+\mathcal{C}\right)I_1(\mathsf{b}) + \left(\mathcal{B} - \frac{3}{\mathsf{b}}\mathcal{C}\right)I_2(\mathsf{b})\right] + \\ & \frac{\pi ik}{2\mathsf{b}^2}\left\{\left[\mathcal{B} + \mathsf{b}\left(\mathcal{A}+\mathcal{C}\right)\right]I_2(\mathsf{b}) + \left[\mathsf{b}\mathcal{B} - 3\mathcal{C}\right]I_3(\mathsf{b})\right\}. \end{aligned} \tag{3.41}$$

Finally, the input power in nondimensional form is given by

$$\begin{aligned} C_P = \frac{P}{\frac{1}{2}\rho U^3 c} = {} & -\Re[\Gamma_0]\times\Re[\mathcal{Q}(\dot{\mathcal{F}},\dot{\mathcal{E}},\dot{\mathcal{D}})] - \Re[\mathcal{H}]\times\Re\left[\Gamma_0 C_1(k)\right] + \Re[\dot{\Gamma}_0]\times\Re[\mathcal{Q}(g_1,g_2,g_3)] - \\ & \Re[\mathcal{A}]\times\Re[\Omega_0(\dot{\mathcal{F}},\dot{\mathcal{E}},\dot{\mathcal{D}})] - \Re[\mathcal{B}]\times\Re[\Omega_1(\dot{\mathcal{F}},\dot{\mathcal{E}},\dot{\mathcal{D}})] - \Re[\mathcal{C}]\times\Re[\Omega_2(\dot{\mathcal{F}},\dot{\mathcal{E}},\dot{\mathcal{D}})] + \\ & \Re[\dot{\mathcal{A}}]\times\Re[\Omega_0(g_1,g_2,g_3)] + \Re[\dot{\mathcal{B}}]\times\Re[\Omega_1(g_1,g_2,g_3)] + \Re[\dot{\mathcal{C}}]\times\Re[\Omega_2(g_1,g_2,g_3)], \end{aligned} \tag{3.42}$$

where a dot denotes the time derivative, and the functions $\mathcal{H}$, g_1, g_2 and g_3 are defined as

$$\mathcal{H} = \frac{e^{\mathsf{b}}}{\mathsf{b}^2}\left\{\left[2\left(1 - \frac{1}{\mathsf{b}}\right) - \mathsf{b}\right]\mathcal{D} + (1-\mathsf{b})\mathcal{E} - \mathsf{b}\mathcal{F}\right\}, \tag{3.43}$$

$$g_1 = \frac{1}{\mathsf{b}^3}\left(2\mathcal{D} + \mathsf{b}(\mathsf{b}\mathcal{F} - \mathcal{E})\right), \quad g_2 = \frac{1}{\mathsf{b}^2}(\mathsf{b}\mathcal{E} - 2\mathcal{D}), \quad g_3 = \frac{\mathcal{D}}{\mathsf{b}}. \tag{3.44}$$

3.3. *Propulsive efficiency*

It is defined as the ratio between the time-averaged power output of the airfoil (thrust force multiplied by the forward speed U) and the time-averaged input power required to drive the airfoil,

$$\eta = \frac{\bar{C}_T}{\bar{C}_P}, \tag{3.45}$$

where the time averaged quantities are defined as

$$\bar{C}_T \equiv \frac{1}{T}\int_t^{t+T} C_T(t)dt, \quad \bar{C}_P \equiv \frac{1}{T}\int_t^{t+T} C_P(t)dt, \tag{3.46}$$

with $T = 2\pi/k$ the nondimensional period of the oscillation. This quantity will be computed explicitly for the particular case discussed below.

4. First oscillation mode of a flexible plate

The special case with $\mathsf{b} = 0$ corresponds to a quadratic flexural motion of a heaving and pitching foil, which is of particular interest because it is equivalent to the first oscillation mode of a flexible foil. The corresponding expressions for the lift, thrust, moment and input power are obtained by making the limit $\mathsf{b} \to 0$ in the above expressions.

For the lift one obtains

$$C_L = \pi \left[\dot{\alpha} + 2p\dot{\delta} - \ddot{h} - a\ddot{\alpha} - \left(p^2 + \frac{1}{4} \right) \ddot{\delta} \right] + \Gamma_0 C(k). \tag{4.1}$$

When $\delta_m = 0$ this expression coincides with the lift coefficient obtained by von Kármán & Sears (1938) using the present impulse theory, and previously by Theodorsen (1935) from a more standard potential flow approach.

For the thrust, the functions $\mathcal{Q}$ and Ω_n becomes

$$\lim_{\mathsf{b}\to 0} \mathcal{Q}(\tilde{a}, \tilde{b}, \tilde{c}) = \frac{i\tilde{b}}{k} C(k) + \left[\left(\frac{1+ik}{k} \right) \tilde{b} + i\tilde{a} + \left(\frac{2+ik}{k} - \frac{2i}{k^2} \right) \tilde{c} \right] \frac{2}{\pi} C_1(k) + \frac{\tilde{c}}{k} C_2(k), \tag{4.2}$$

$$\lim_{\mathsf{b}\to 0} \Omega_0(\tilde{a}, \tilde{b}, \tilde{c}) = \tilde{b}\pi, \quad \lim_{\mathsf{b}\to 0} \Omega_1(\tilde{a}, \tilde{b}, \tilde{c}) = \tilde{c}\frac{\pi}{4}, \quad \lim_{\mathsf{b}\to 0} \Omega_2(\tilde{a}, \tilde{b}, \tilde{c}) = \tilde{b}\frac{\pi}{4}, \tag{4.3}$$

where $C_2(k)$ is given by

$$C_2(k) \equiv \frac{H_2^{(2)}(k)}{iH_0^{(2)}(k) + H_1^{(2)}(k)} = F_2(k) + iG_2(k). \tag{4.4}$$

Consequently, the thrust coefficient can be written as

$$\begin{aligned} C_T = {} & -\Re\left[\alpha + 2p\delta\right] \times C_L + \frac{\pi}{2} \left\{ \Re[\delta] \times \Re\left[\frac{\ddot{\alpha}}{2} + p\ddot{\delta} - \dot{\delta} \right] + \Re[\dot{\delta}] \times \Re\left[\frac{\dot{\alpha}}{2} + p\dot{\delta} - \delta \right] \right\} + \\ & \Re\left[\dot{\alpha} + 2p\dot{\delta} \right] \times \Re\left\{ \pi \left[\dot{h} + a\dot{\alpha} + \left(p^2 + \frac{1}{4} \right) \dot{\delta} - (\alpha + 2p\delta) \right] + \Gamma_0 \left[\frac{i}{k} C + \left(\frac{1+ik}{k} \right) \frac{2}{\pi} C_1 \right] \right\} + \\ & \Re\left[\dot{h} + a\dot{\alpha} - (\alpha + 2p\delta) + p^2\dot{\delta} \right] \times \Re\left[\Gamma_0 \frac{-2i}{\pi} C_1 \right] + \Re[\delta] \times \Re\left[\Gamma_0 \left(-iC_2 - 2\frac{1+ik}{k} \frac{2}{\pi} C_1 \right) \right] + \\ & \Re[\dot{\delta}] \times \Re\left\{ \Gamma_0 \left[\left(\frac{2i}{k^2} - \frac{2+ik}{k} \right) \frac{2}{\pi} C_1 - \frac{C_2}{k} \right] \right\}. \end{aligned} \tag{4.5}$$

The complex form of this expression coincides with the thrust obtained by Fernandez-Feria (2016) when $\delta_m = 0$, though here the real part of the nonlinear expression is separated in a slightly different form.

The moment coefficient becomes

$$\begin{aligned} C_M = {} & \frac{\Gamma_0}{2} \left(\frac{1}{2} + a \right) C(k) - \frac{\pi}{2} \left\{ \left(\frac{1}{2} - a \right) \dot{\alpha} + a\ddot{h} + \left(\frac{1}{8} + a^2 \right) \ddot{\alpha} + \right. \\ & \left. \left[\frac{p}{4} + a\left(p^2 + \frac{1}{4} \right) \right] \ddot{\delta} + \left[\left(\frac{1}{2} - a \right) p - 1 \right] \frac{\dot{\delta}}{2} - \delta \right\}. \end{aligned} \tag{4.6}$$

As in the case of the lift, the above expression coincides with the moment obtained by von Kármán & Sears (1938) when $\delta_m = 0$.

Finally, the input power coefficient can be written in the physically relevant form

$$C_P = -\dot{h}(t) C_L - 2\dot{\alpha}(t) C_M - \dot{\delta}(t) \Upsilon, \tag{4.7}$$

where

$$\Upsilon = p\left(4C_{Mp} - pC_L\right) + \Gamma_0 C(k) - \frac{\pi}{4} \left[\ddot{h} + a\ddot{\alpha} + \left(p^2 + \frac{1}{3} \right) \ddot{\delta} - 2\delta \right], \tag{4.8}$$

and $C_{Mp} \equiv C_M(a = p)$ is the moment coefficient but in relation to the point $x = p$, where the

flexure component of the motion vanishes. It must be noted that, to obtain the above input power coefficient, the limit $\mathsf{b} \to 0$ in the double integral appearing in (3.13), which now can be written as

$$\int_{-1}^{1} \left(\int_{x}^{1} \frac{\partial z_s}{\partial t} d\xi \right) \frac{\partial \varpi_s}{\partial t} dx = \int_{-1}^{1} \left[\mathcal{H} + \left(g_1 + g_2 x + g_3 x^2 \right) e^{\mathsf{b}x} \right] \frac{\partial \varpi_s}{\partial t} dx, \tag{4.9}$$

has to be done collectively to all the terms inside the integrand, because the functions $\mathcal{H}, g_1, g_2$ and g_3 diverge separately as $\mathsf{b} \to 0$, but together

$$\lim_{\mathsf{b}\to 0} \left[\mathcal{H} + \left(g_1 + g_2 x + g_3 x^2 \right) e^{\mathsf{b}x} \right] = \mathcal{F}(x-1) + \frac{\mathcal{E}}{2} \left(x^2 - 1 \right) + \frac{\mathcal{D}}{3} \left(x^3 - 1 \right). \tag{4.10}$$

Thus, the general expression (3.42) is valid when $\mathsf{b} \neq 0$, and one has to use the expression (4.7) when $\mathsf{b} = 0$.

4.1. *Time-averaged coefficients and propulsive efficiency*

The time-averaged coefficients (3.46) can now be written in simple closed forms. To that end it is convenient to define the following nondimensional parameters to separate the different components of the foil's motion:

$$\theta = \frac{a_0}{k h_0}, \quad \theta_{hd} = \frac{\delta_m}{k h_0}, \quad \theta_{pd} = \frac{\delta_m}{a_0}, \tag{4.11}$$

where the first one, θ, is the well-known feathering parameter (Lighthill 1969) for a pitching and heaving motion of a rigid foil. Thus, the time-averaged thrust coefficient can be written either normalized in relation to a pure heaving motion,

$$\begin{aligned} \hat{C}_{Th} \equiv \frac{\bar{C}_T}{(k h_0)^2} = t_h(k) + t_{hp}(k,a,\phi)\theta + t_p(k,a)\theta^2 + \\ t_{hd}(k,p,\psi)\theta_{hd} + t_{pd}(k,p,a,\psi,\phi)\theta_{hd}\theta + t_d(k,p)\theta_{hd}^2, \end{aligned} \tag{4.12}$$

or in relation to a pure pitching motion,

$$\begin{aligned} \hat{C}_{Tp} \equiv \frac{\bar{C}_T}{a_0^2} = t_h(k)\theta^{-2} + t_{hp}(k,a,\phi)\theta^{-1} + t_p(k,a) + \\ t_{hd}(k,p,\psi)\theta_{pd}\theta^{-1} + t_{pd}(k,p,a,\psi,\phi)\theta_{pd} + t_d(k,p)\theta_{pd}^2, \end{aligned} \tag{4.13}$$

where the functions $t_h(k)$, $t_{hp}(k,a,\phi)$, $t_p(k,a)$, $t_{hd}(k,p,\psi)$, $t_{pd}(k,a,p,\phi,\psi)$ and $t_d(k,p)$ are given by Eqs. (A 1)-(A 6) in the Appendix. Note that for $\theta_{hd} = 0$ or $\theta_{pd} = 0$ these expressions does not coincide exactly with those for an oscillating rigid foil given in Fernandez-Feria (2017) because here the real part of the complex nonlinear expression for the thrust force is separated in a slightly different way, but the results are practically indistinguishable.

The time-averaged input power coefficient is given by

$$\bar{C}_P = -\overline{\dot{h}(t) C_L} - 2\overline{\dot{\alpha}(t) C_M} - \overline{\dot{\delta}(t) \Upsilon}, \tag{4.14}$$

which, similarly to the mean thrust coefficient, can be written in terms of the parameters (4.11) either as

$$\begin{aligned} \hat{C}_{Ph} \equiv \frac{\bar{C}_P}{(k h_0)^2} = p_h(k) + p_{hp}(k,a,\phi)\theta + p_p(k,a)\theta^2 + \\ p_{hd}(k,p,\psi)\theta_{hd} + p_{pd}(k,p,a,\psi,\phi)\theta_{hd}\theta + p_d(k,p)\theta_{hd}^2, \end{aligned} \tag{4.15}$$

or as

$$\begin{aligned} \hat{C}_{Pp} \equiv \frac{\bar{C}_P}{a_0^2} = p_h(k)\theta^{-2} + p_{hp}(k,a,\phi)\theta^{-1} + p_p(k,a) + \\ p_{hd}(k,p,\psi)\theta_{pd}\theta^{-1} + p_{pd}(k,p,a,\psi,\phi)\theta_{pd} + p_d(k,p)\theta_{pd}^2, \end{aligned} \tag{4.16}$$

where the functions $p_h(k)$, $p_{hp}(k,a,\phi)$, $p_p(k,a)$, $p_{hd}(k,p,\psi)$, $p_{pd}(k,a,p,\phi,\psi)$ and $p_d(k,p)$ are given by Eqs. (A 7)-(A 12) in the Appendix.

Finally, the propulsive efficiency (3.45) can be computed using any of the above alternative forms of $\bar{C}_T$ and $\bar{C}_P$. It is convenient to use a propulsive efficiency relative to that of a rigid oscillating

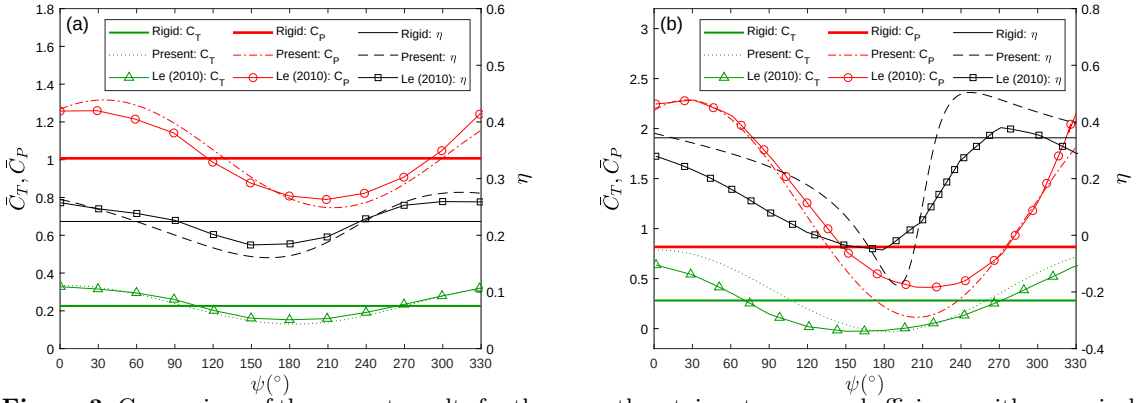

Figure 3: Comparison of the present results for the mean thrust, input power and efficiency with numerical results from Le *et al.* (2010) for a pure heaving motion with deflection ($\mathsf{b} = a_0 = 0$). $h_0 = 0.35$, $k = 1.82$, $p = -1$, $C_{T0} = -0.055$. (a) $\delta_m = 0.1$, $\Delta t/T = -0.06$ for $\bar{C}_P$. (b) $\delta_m = 0.4$, $\Delta t/T = -0.025$ for $\bar{C}_P$.

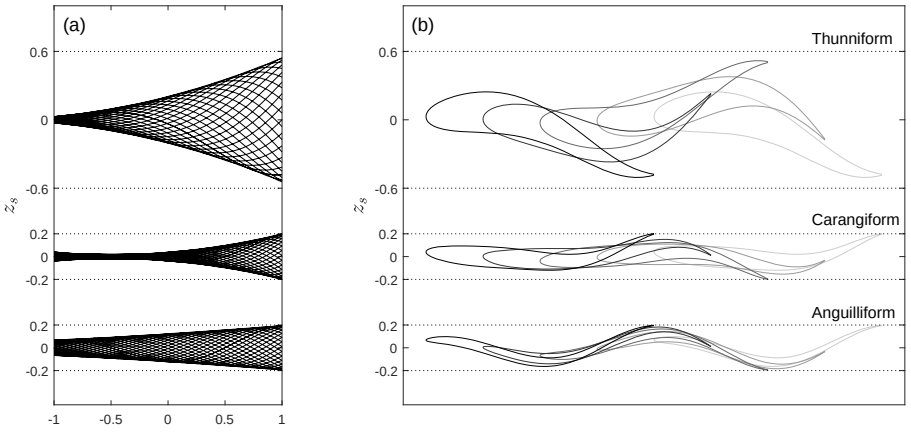

Figure 4: (a) Anguilliform, carangiform and thunniform motion at its mid-line. (b) Superimposed body outlines separated by $\Delta t/T = 0.25$. The corresponding values of the parameters in the present model and references are given in Table 1.

foil, η_0,

$$\hat{\eta} \equiv \eta - \eta_0, \quad \text{with} \quad \eta_0 = \frac{t_h(k) + t_{hp}(k,a,\phi)\theta + t_p(k,a)\theta^2}{p_h(k) + p_{hp}(k,a,\phi)\theta + p_p(k,a)\theta^2}. \tag{4.17}$$

5. Model validation

Before analysing with detail the results corresponding to the first oscillation mode of a flexible foil ($\mathsf{b} = 0$) considered in the previous section, it is convenient to validate the present theoretical results by comparing them with available numerical data for both $\mathsf{b} = 0$ and $\mathsf{b} \neq 0$.

We first consider the numerical results by Le *et al.* (2010), who investigated the performance of a flapping wing with different chord flexures, corresponding, in the notation of the present model, to $\mathsf{b} = 0$ and $a_0 = 0$ (no pitching motion). These authors reported results for different values of the flexure amplitude δ_m and the heave amplitude h_0, with varying phase shift ψ between the two components of the foil's motion. In particular, they considered the case of a plunging NACA0012 foil clamped at the leading edge (i.e., with $p = -1$ in our notation and without rotation at the leading edge) for $Re = 3 \times 10^4$.

Figure 3 compares the numerical results by Le *et al.* (2010) for the mean values of the thrust and input power coefficients, and for the propulsive efficiency, as functions of the phase shift ψ between the heaving and deflection motions, with the present theoretical results for two values of δ_m. For reference sake the results for a rigid foil are also included, which, are obviously independent of ψ. The agreement is quite good for the three mean magnitudes represented in all the range of values of ψ. But it should be noted that, since the computation of the input power is very sensitive to

	h_0	a	a_0	ϕ	p	δ_m	ψ	b_1	b_2	k	Re
Anguilliform	0	0	0	0	-3,8243	0,1960	0	0	π	$[0.5,\ 2]\pi$	5000
	0.6346	4.1730	0.1212	π	0	0	0	0	π	$[0.3,1.3]\pi$	$[50, 2\cdot 10^5]$
Carangiform	0,01906	0	0	0	-0,4923	0,18094	0	0	π	$[0.5,\ 2]\pi$	5000
	0,1	0	0	0	0	0	0	0.25	π	π & 2.5π	100
Thunniform	0	0	0	0	-1.586	0.5549	0.1317	0	$\pi/1.67$	$[0.5,\ 2]\pi$	$7.1[10^3, 10^5]$

Table 1: Values of the kinematic parameters for the different motions considered in Figs. 4-6. Anguilliform from Tytell (2004) and Zhang *et al.* (2018), respectively; carangiform from Dong & Lu (2007) and Zhang & Eldredge (2009), respectively; and thunniform from Chang *et al.* (2012).

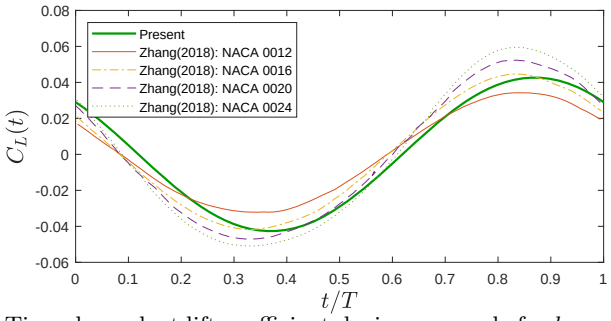

Figure 5: Anguilliform. Time-dependent lift coefficient during one cycle for $k = \pi$. Numerical results from Fig. 9(d) in Zhang *et al.* (2018) for $Re = 5 \times 10^4$. Note that these authors nondimensionalize the lift as $L/(\rho U^2 c^2)$, so that the present $C_L/4$ is plotted. The corresponding values of the kinematic parameters in the present model are given in Table 1.

any temporal shift between the lift coefficient $C_L(t)$ obtained numerically and the vertical motion $\dot{h}(t)$, to fit $\bar{C}_P$ we have included a very small temporal shift Δt in the lift when computing the mean value of C_P from our theoretical formulation as follows

$$\bar{C}_P = -\frac{1}{T}\int_t^{t+T} \left[\dot{h}(t) C_L(t+\Delta t) + \dot{\delta}(t)\Upsilon(t)\right] dt. \tag{5.1}$$

The values of Δt are given in the caption of Fig. 3, together with all the kinematic parameters. In Fig. 3(b) Δt is taken directly from $C_L(t)$ data in Le *et al.* (2010), which are not available for the case of Fig. 3(a), and we take the value that best fit C_P. These Δt are very small compared with the period T, justifying their use to compensate any small temporal shift in the computation of C_L from the numerical simulations. Note also the excellent agreement between the theoretical results for $\bar{C_T}$ with the numerical results obtained by Le *et al.* (2010) for any value of ψ, particularly in Fig. 3(a) where the nondimensional flexure amplitude δ_m is smaller.

Next we consider the numerical results by Zhang *et al.* (2018) and by Dong & Lu (2007), who analyse two different undulatory motions, i.e., with $\mathsf{b} \neq 0$ in the present notation. As commented on in the Introduction, this kind of motion is commonly used to model fish locomotion. To put them into a biological context, the body or caudal fin of fishes can be classified into five groups that differ in the fraction of their body that is displaced laterally (coordinate z in the present notation) (Breder 1926): anguilliform (e.g. eels), sub-carangiform (e.g. trout), carangiform (e.g. jack mackerels), thunniform (e.g. tunas), and ostraciiform (e.g. boxfishes). Examples of three of these motions are plotted in Fig.4, with the corresponding values of the parameters in the present model given in Table 1. Also included are the values of the parameters corresponding to the selected numerical results by Zhang *et al.* (2018) and Dong & Lu (2007), which are compared below with the present theoretical results, together with other references and some additional information about the numerical simulations.

Figure 5 compares the lift coefficient from the numerical results by Zhang *et al.* (2018) for

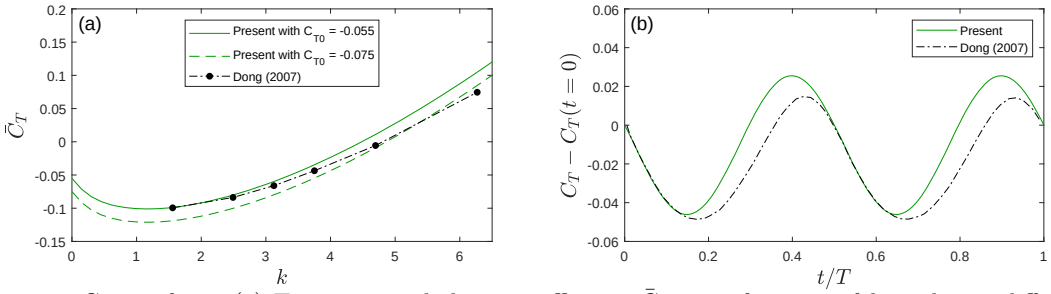

Figure 6: Carangiform. (a) Time-averaged thrust coefficient, $\bar{C}_T$, as a function of k, with two different values of the offset drag, $\bar{C}_{T0} = -0.055$ and -0.075. (b) Time-dependent thrust coefficient during one cycle for $k = 1.5\pi$. Numerical results from Dong & Lu (2007). The corresponding values of the kinematic parameters in the present model are given in Table 1.

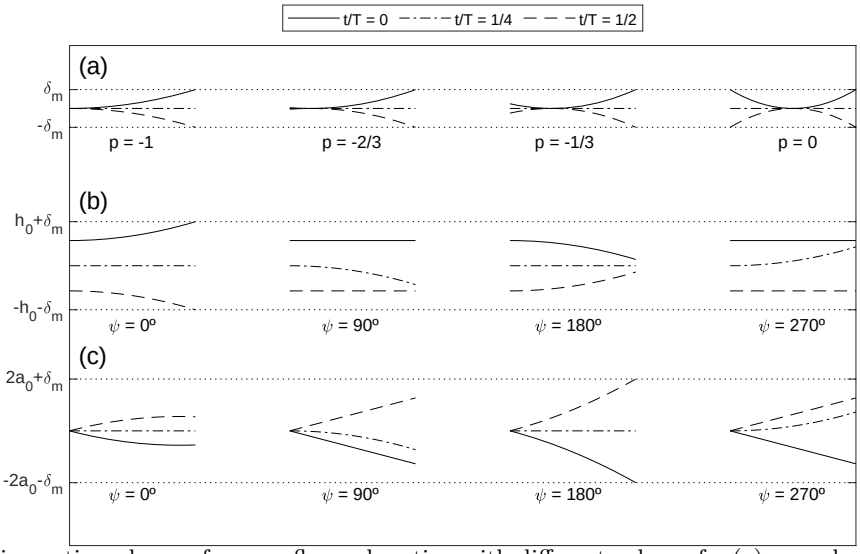

Figure 7: Kinematics schemes for pure flexural motion with different values of p (a), pure heaving motion with chordwise deflection for different values of ψ and $p = -1$ (b), and pure pitching motion with chordwise deflection for different values of ψ and $p = -1$ (c). In all cases the same three instants of time are plotted, as indicated.

several NACA profiles with the present theoretical results. The numerical results for the different foil thicknesses are all quite close to each other, and with a good agrement with the present zero-thickness theoretical results, with a slightly better agreement for the NACA0016 profile, but for no particular reason.

Figure 6 compares the thrust coefficient computed numerically by Dong & Lu (2007) with the present theoretical results, both the time-averaged values as a function of the reduced frequency k, and its temporal evolution during one cycle for $k = 1.5\pi$. As discussed in Fernandez-Feria (2017), the mean values are corrected to account for the viscous drag by adding to the present theoretical results a quasi-static thrust $\bar{C}_{T0} < 0$ (i.e., by subtracting an offset quasi-static drag $-\bar{C}_{T0}$), corresponding to the numerical results for $k = 0$. Since these authors do not provide numerical results for $k = 0$, we have selected two values of $\bar{C}_{T0}$ in Fig. 6(a), one that yields a better fit for small values of k and the other one for higher values of k, though both values of $\bar{C}_{T0}$ are quite close to each other. Notice that no mean drag correction is needed in Fig. 6(b) since we plot the instantaneous thrust coefficient minus its numerical value at $t = 0$, $C_T(t = 0)$.

6. Results and discussion for $\mathsf{b} = 0$

Results with no undulatory motion ($\mathsf{b} = 0$) are presented and discussed in this section. The kinematics of the three different cases considered are sketched in Fig. 7.

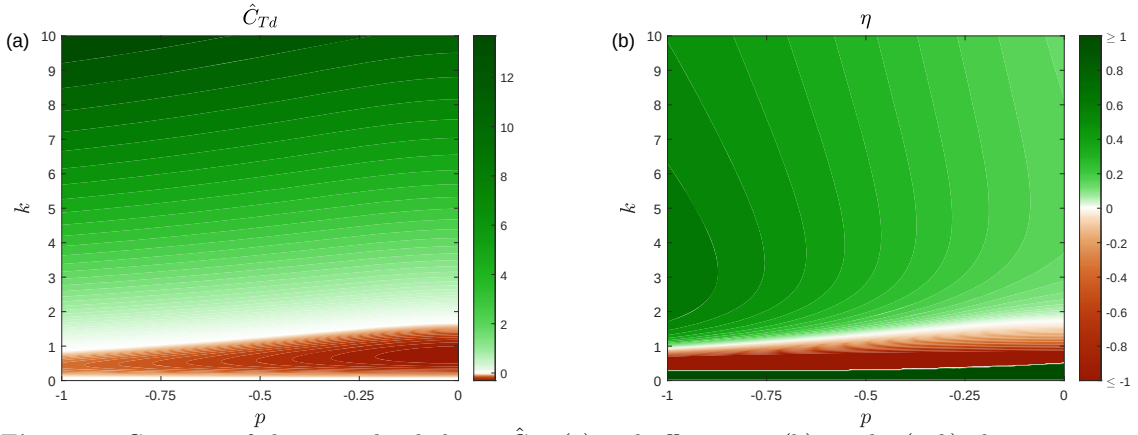

Figure 8: Contours of the normalized thrust $\hat{C}_{Td}$ (a) and efficiency η (b) on the (p, k)-plane in a pure flexural motion ($\mathsf{b} = h_0 = a_0 = 0$).

6.1. *Pure flexural motion*

We consider first the simplest case of a pure flexural motion of the first oscillating mode, without heaving or pitching motions ($h_0 = 0$ and $a_0 = 0$). Note from equations (4.12) and (4.15) that in this case only the last terms of the thrust and power coefficients are different from zero, which are quadratic in the trailing-edge deflection amplitude δ_m. Thus, it is convenient to use the following normalized thrust and power coefficients:

$$\hat{C}_{Td} \equiv \frac{\bar{C}_T}{\delta_m^2} = t_d(k,p), \quad \hat{C}_{Pd} \equiv \frac{\bar{C}_P}{\delta_m^2} = p_d(k,p), \tag{6.1}$$

where the functions t_d and p_d are given in the Appendix. The efficiency is $\eta = t_d(k,p)/p_d(k,p)$.

Figure 8 shows the contours of the normalized thrust $\hat{C}_{Td}$ and efficiency η as k and the location of the deflection pivot point p are varied. It is clear from this figure that no thrust is generated when $k \lesssim 1$ (i.e., $\hat{C}_{Td} < 0$). For $k \gtrsim 1$, the maximum propulsive efficiency is always reached for a clamped leading edge ($p = -1$). This can be justified by the consideration that in this case all the bending of the foil is useful to generate thrust [see Fig. 7(a)]. For this reason we only consider the cases with $p = -1$ in the results reported below when a heaving or a pitching motion is added to the flexural motion. The optimum value of the reduced frequency k in terms of propulsive efficiency for $p = -1$ is about 3.

6.2. *Pure heaving motion with chordwise deflection*

Next in complexity is the case of a pure heaving motion combined with a deflection motion of the foil, i.e., the first oscillation mode of a flexible airfoil for a pure heaving motion, for which (4.12) and (4.15) become

$$\hat{C}_{Th} = t_h(k) + t_{hd}(k,p,\psi)\theta_{hd} + t_d(k,p)\theta_{hd}^2, \tag{6.2}$$

$$\hat{C}_{Ph} = p_h(k) + p_{hd}(k,p,\psi)\theta_{hd} + p_d(k,p)\theta_{hd}^2, \tag{6.3}$$

with the ratio θ_{hd} between the deflection and heaving amplitudes defined by equation (4.11) and the different functions given in the Appendix. To compare the thrust of the flexible foil with the thrust generated by its rigid counterpart, we define a normalized thrust as

$$\hat{C}_{Th}^* = \frac{\hat{C}_{Th}}{t_h(k)}, \tag{6.4}$$

which only depends on the nondimensional parameters k, p, ψ and θ_{hd}, as it does the normalized efficiency $\hat{\eta}$ defined in Eq. (4.17). In order to reduce further the number of parameters we focus on the case of a clamped leading edge, i.e, $p = -1$, which was shown in §6.1 to yield the best propulsion efficiency.

Figure 9 shows the contours of the normalized thrust $\hat{C}_{Th}^*$ and efficiency $\hat{\eta}$ as k and ψ are varied with $\theta_{hd} = 0.75$. It is observed that, for $1 \lesssim k \lesssim 4$, the flexible foil generates more thrust than the rigid airfoil ($\hat{C}_{Th}^* > 1$) when $250^\circ \lesssim \psi \lesssim 100^\circ$, and less when $100^\circ \lesssim \psi \lesssim 250^\circ$. In fact, a phase

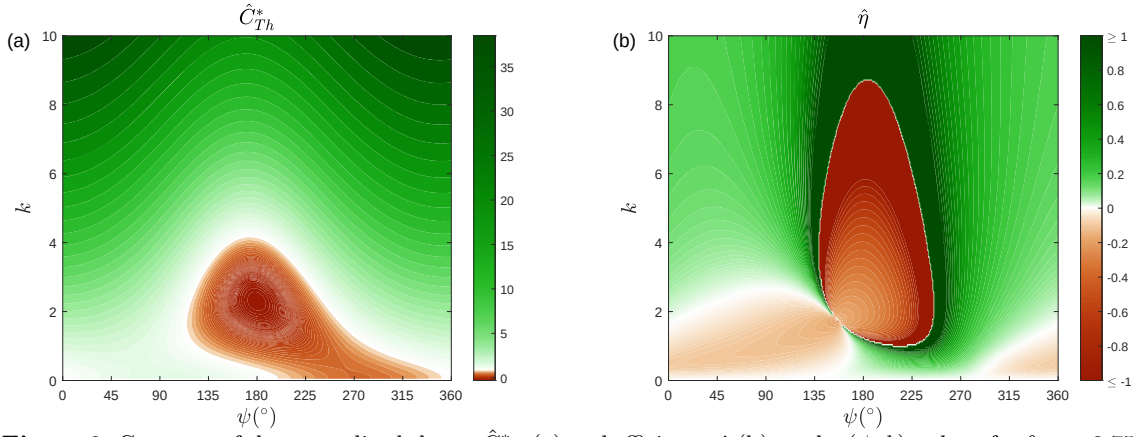

Figure 9: Contours of the normalized thrust $\hat{C}^*_{Th}$ (a) and efficiency $\hat{\eta}$ (b) on the $(\psi, k)-$plane for $\theta_{hd} = 0.75$ and $p = -1$ in a pure heaving and deflection motion ($\mathsf{b} = \theta = \theta_{pd} = 0$).

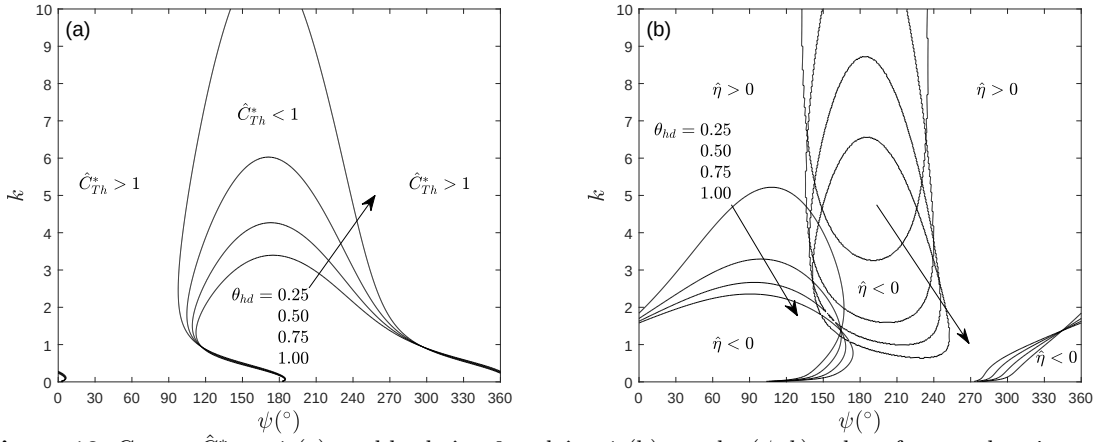

Figure 10: Curves $\hat{C}^*_{Th} = 1$ (a), and both $\hat{\eta} = 0$ and $\hat{\eta} = 1$ (b), on the $(\psi, k)-$plane for pure heaving and deflection motion ($\mathsf{b} = \theta = \theta_{pd} = 0$) with $0 < \theta_{hd} \leqslant 1$ and $p = -1$.

shift ψ between 100° and 250°, approximately, corresponds to a motion of the foil with the trailing edge pointing downwards at the beginning of the downstroke, and opposite at the beginning of the upstroke [see Fig. 7(b)], generating less thrust than its rigid counterpart. In relation to the efficiency, Fig.9(b) shows that the model yields a singularity for a particular combination of k and ψ due to the vanishing of the power coefficient in the present model, where η changes from $+\infty$ to $-\infty$), so that it is expected that close to this curve on the $(\psi, k)-$plane the propulsive efficiency reaches a local maximum, greatly enhancing the propulsive efficiency of a rigid heaving foil. For k of order unity this corresponds, approximately, to ψ between 250° and 270°.

To see the effect of θ_{hd} we plot the curves on the $(\psi, k)-$plane corresponding to $\hat{C}^*_{Th} = 1$ in Fig. 10(a), and both the curves corresponding to $\hat{\eta} = 0$ and $\hat{\eta} = 1$ (i.e., close to the singularity) in Fig. 10(b), for $0 < \theta_{hd} \leqslant 1$. Figure 10(a) shows that the regions of enhanced and reduced thrust in relation to a heaving rigid foil remain almost independent of θ_{hd} for k of order unity. For the efficiency [Fig. 10(b)] the situation is somewhat similar, but the singularity moves towards smaller values of k as θ_{hd} increases. Thus, the present model predicts a maximum enhancement of the propulsive efficiency in relation to a rigid heaving foil when $k \approx 1$ for θ_{hd} approacing unity and $\psi \approx 260^o$. This result is in qualitative agreement with the experimental results of Ramananarivo *et al.* (2011) for a similar foil motion, where the maximum efficiency is found to be reached when the trailing-edge deflection angle is approximately equal to the effective angle of attack at the mid-downstroke, which is the situation for ψ approaching 270^o in Fig. 7(b).

6.3. *Pure pitching motion with chordwise deflection*

As the third simple case we consider a pure pitching motion combined with a deflection motion of the foil, i.e., the first oscillation mode of a flexible airfoil for pure pitching motion, for which (4.13)

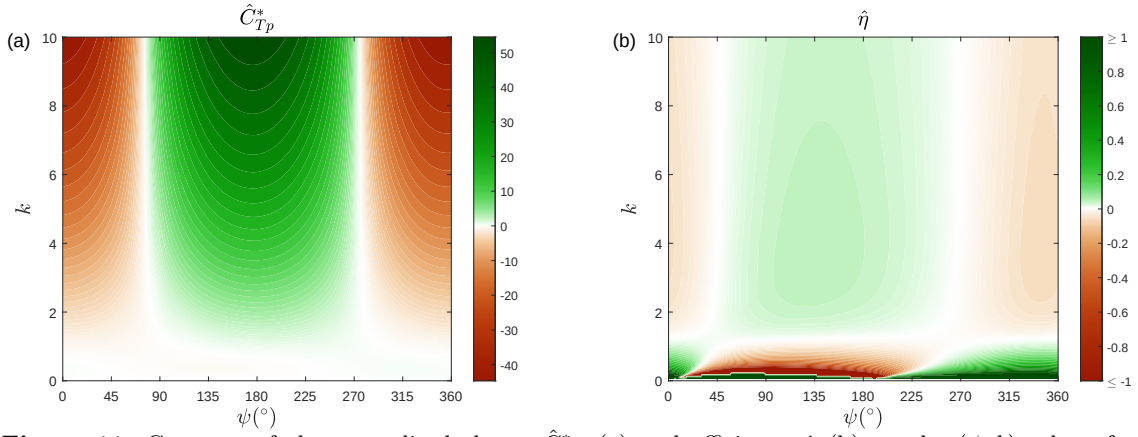

Figure 11: Contours of the normalized thrust $\hat{C}^*_{Tp}$ (a) and efficiency $\hat{\eta}$ (b) on the $(\psi, k)-$plane for $\theta_{pd} = 0.75$ and $a = p = -1$ in a pure pitching and deflection motion ($\mathsf{b} = \theta^{-1} = \theta_{hd} = 0$).

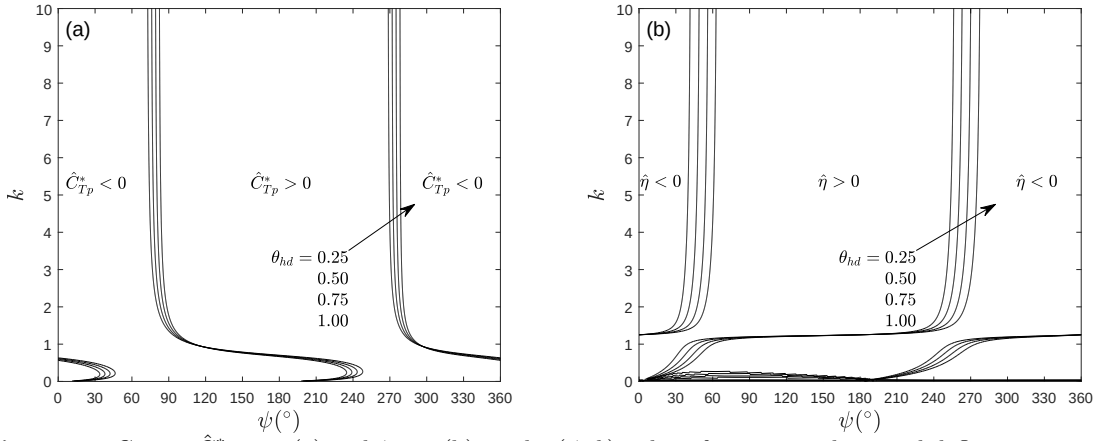

Figure 12: Curves $\hat{C}^*_{Tp} = 0$ (a) and $\hat{\eta} = 0$ (b) on the $(\psi, k)-$plane for pure pitching and deflection motion ($\mathsf{b} = \theta^{-1} = \theta_{hd} = 0$) with $0 < \theta_{pd} \leqslant 1$ and $a = p = -1$.

and (4.16) become

$$\hat{C}_{Tp} = t_p(k, a) + t_{pd}(k, p, a, \psi, \phi)\theta_{pd} + t_d(k, p)\theta^2_{pd}, \tag{6.5}$$

$$\hat{C}_{Pp} = p_p(k, a) + p_{pd}(k, p, a, \psi, \phi)\theta_{pd} + p_d(k, p)\theta^2_{pd}, \tag{6.6}$$

with the ratio θ_{pd} between the deflection and pitching amplitudes defined in equation (4.11). Since the thrust of a rigid plate may change its sign for a pure pitching motion, to avoid singularities it is convenient to redefine the normalized thrust coefficient in this case as

$$\hat{C}^*_{Tp} = \hat{C}_{Tp} - t_p(k, a). \tag{6.7}$$

Now $\hat{C}^*_{Tp} = 0$ means the same thrust coefficient as the equivalent pitching rigid foil. The definition of the normalized efficiency (4.17) does not change. Both $\hat{C}^*_{Tp}$ and $\hat{\eta}$ depend on the nondimensional parameters k, a, p, ψ and θ_{pd} (note that one may set $\phi = 0$ since there is no heaving motion, and ψ is now the phase shift of the deflection in relation to the pitch). Similarly to the previous case, to reduce the number of parameters we focus on a deflection pivoting at the leading edge ($p = -1$), which in the present case implies also a pitching motion about the leading edge, i.e., $a = p = -1$.

Figure 11 shows the contours of the normalized thrust $\hat{C}^*_{Tp}$ and efficiency $\hat{\eta}$ on the $(\psi, k)-$plane for $\theta_{pd} = 0.75$. For the thrust [Fig. 11(a)] we can distinguish two regions: one for small k with two maxima of the relative thrust, around $\psi = 0°$ and for $\psi \gtrsim 270°$, and another region for $k \gtrsim 1$ where the enhanced thrust is for $90° \lesssim \psi \lesssim 270°$. Figure 11(b) shows that these regions approximately coincide with those of enhanced efficiency.

The effect of θ_{pd} is plotted in Fig. 12 as curves corresponding to $\hat{C}^*_{Tp} = 0$ and $\hat{\eta} = 0$ on the $(\psi, k)-$plane for $0 < \theta_{pd} \leqslant 1$. The regions of enhanced and reduced thrust in relation to a pitching rigid foil are nearly independent of θ_{pd}, with larger variations as k increases. However, in contrast to

the pure heaving motion, the regions of positive and negative relative efficiency $\hat{\eta}$ remain practically unchanged as θ_{pd} varies from zero to unity [Fig. 12(b)]. Therefore, the above discussed region of maximum enhancement in the propulsive efficiency of a flexible foil in relation to a pitching rigid foil about its leading edge remain practically independent of the trailing edge deflection amplitude in relation to the pitch amplitude, within the present linearized potential theory valid for small amplitudes.

7. Concluding remarks

The closed expressions obtained in the present work for the aerodynamic force components and moment on a two-dimensional flexible foil undergoing a quite general undulatory motion, which are validated against available numerical results for sufficiently high Reynolds numbers and small amplitude of the oscillations, constitute a convenient tool for predicting and evaluating the optimal conditions for propulsion in terms of thrust generation and efficiency in a wide range of animal and bioinspired robotic locomotion.

Relatively simple analytic expressions are obtained for the interesting cases of pitching and heaving motions superimposed to a chordwise flexibility of the foil, with the additional force and moment terms in relation to an oscillating rigid foil neatly separated, and characterized by the ratio between the amplitudes of the deflection and the rigid motions. When this nondimensional parameter vanishes one recovers previous results for a pitching and heaving rigid foil. A detailed evaluation of the propulsion performance is made for these particular cases, mapping the regions of thrust and of propulsive efficiency enhancement in relation to the rigid foil counterpart in the parameter space of the reduced frequency and the relevant deflection parameters.

The present results are limited to small amplitudes of the oscillations and sufficiently high Reynolds number for which the linearized potential theory applies. In addition, no analysis is made about the fluid-structure interaction that may produce the particular deflection or undulatory motion of the foil. Previous works that have analysed this fluid-structure interaction have shown that, in some particular pitching and heaving motions of the foil, the regions of optimal propulsion are related to structural resonant frequencies of the foil (Michelin & Llewellyn Smith 2009; Dewey *et al.* 2013; Moore 2014; Paraz *et al.* 2016; Moore 2017). The present analytical results are independent of the material properties of the foil, depending only on the prescribed kinematics of the flexible foil. Although to analyse the fluid-structure interaction one needs to model a truly general motion of the deformable foil, with infinite kinematic parameters, as recently done numerically in this limit of linear potential theory by Tzezana & Breuer (2019), we believe that with the present fairly broad class of flapping undulatory motion, with nine nondimensional parameters, one may undertake a similar, but more limited, analysis of the fluid-structure interaction to obtain approximately these kinematics parameters for given properties of the flexible or compliant material and the boundary conditions at the leading and trailing edges, with the advantage that now the aerodynamic force and moment are obtained analytically in terms of these parameters from a general impulse theory. This is left for future research.

Acknowledgments

This research has been supported by the *Ministerio de Ciencia, Innovación y Universidades* of Spain Grant No. DPI2016-76151-C2-1-R.

Appendix A. Functions for the time-averaged coefficients

For easy reference, the functions $t_h(k)$, $t_{hp}(k,a,\phi)$,$t_p(k,a)$,$t_{hd}(k,p,\psi)$,$t_{pd}(k,a,p,\phi,\psi)$ and $t_d(k,p)$ appearing in the time-averaged thrust coefficient, $\hat{C}_{Th}$ or $\hat{C}_{Tp}$, are reproduced here. These functions can be written as

$$t_h(k) = -2G_1(k), \tag{A 1}$$

$$t_{hp}(k,a,\phi) = [(3-4a)G_1 k - 2F_1]\cos(\phi) + (2G_1 - F_1 k)\sin(\phi), \tag{A 2}$$

$$t_p(k,a) = 2(1-a)k\left[F_1 - \left(\frac{1}{2}-a\right)G_1 k\right], \tag{A 3}$$

$$t_d(k,p) = \frac{k}{(1-p)^2}\left\{4F_1\left(\frac{1}{2}-p\right) - G_1 k[1+2(p-1)p]\right\}, \tag{A 4}$$

$$t_{hd}(k,p,\psi) = \frac{4}{(1-p)^2}\left(p-\frac{1}{2}\right)\left(G_1 - \frac{F_1 k}{2}\right)\sin(\psi) + \frac{4}{(1-p)^2}\left\{F_1\left(\frac{1}{2}-p\right) - G_1 k\left[\left(p-\frac{3}{2}\right)p+\frac{3}{4}\right]\right\}\cos(\psi), \tag{A 5}$$

$$t_{pd}(k,a,p,\phi,\psi) = \frac{4k}{(1-p)^2}\left\{F_1\left[a\left(\frac{1}{2}-p\right)+2\left(1-\frac{p}{4}\right)p-1\right] + G_1 k\left[\left(\frac{3}{4}-a\right)p^2+\frac{3}{2}a\left(p-\frac{1}{2}\right)-p+\frac{1}{2}\right]\right\}\cos(\phi-\psi) \frac{k}{(1-p)^2}\left[2a\left(\frac{1}{2}-p\right)+p^2\right](2G_1 - F_1 k)\sin(\phi-\psi). \tag{A 6}$$

Finally, the functions $p_h(k), p_{hp}(k,a,\phi), p_p(k,a), p_{hd}(k,p,\psi), p_{pd}(k,a,p,\phi,\psi)$ and $p_d(k,p)$ appearing in the time-averaged input power coefficient, $\hat{C}_{Ph}$ or $\hat{C}_{Pp}$, can be written as

$$p_h(k) = \pi F, \tag{A 7}$$

$$p_{hp}(k,a,\phi) = -\pi\left\{\left[2k\left(\frac{1}{4}-aF\right)+G\right]\cos(\phi) + (F-Gk)\sin(\phi)\right\}, \tag{A 8}$$

$$p_p(k,a) = -\pi k^2\left\{\left(\frac{1}{4}-a^2\right)F + \frac{1}{2}\left(a-\frac{1}{2}\right) + \left(a+\frac{1}{2}\right)\frac{G}{k}\right\}, \tag{A 9}$$

$$p_d(k,p) = \frac{k\pi}{(1-p)^4}\left\{\frac{Fk}{2}\left[p\left(2p^3+p-1\right)+1\right] - G\left[p\left(2p^2+p+1\right)-1\right] + \frac{kp}{2}\left[p\left(p+\frac{1}{2}\right)-1\right]\right\}, \tag{A 10}$$

$$p_{hd}(k,p,\psi) = \frac{2\pi}{(1-p)^2}\left\{\left[Fk\left(p^2+\frac{3}{4}\right) + G\left(\frac{1}{2}-p\right) - \frac{kp}{2}\right]\cos(\psi) + \left[F\left(\frac{1}{2}-p\right) + Gk\left(p+\frac{1}{4}\right)\right]\sin(\psi)\right\}, \tag{A 11}$$

$$p_{pd}(k,a,p,\phi,\psi) = \frac{k\pi}{(1-p)^2}\left\{F\left[-2a\left(\frac{1}{2}-p\right)-p^2-\frac{3}{2}\right] + Gk\left[-2a\left(p+\frac{1}{4}\right)+p^2+\frac{3}{4}\right] + k^2p^2(a-p)+\frac{1}{2}\right\}\sin(\phi-\psi) - \frac{k\pi}{(1-p)^2}\left\{Fk\left[\frac{1}{4}-2ap^2-\frac{3a}{2}+p\right] + G\left[2a\left(p-\frac{1}{2}\right)+p(p+2)+\frac{1}{2}\right] + \frac{kp}{2}\left(\frac{a}{2}+p-\frac{5}{4}\right)+\frac{k}{4}\right\}\cos(\phi-\psi). \tag{A 12}$$

REFERENCES

Alben, S. 2008 Optimal flexibility of a flapping appendage in an inviscid fluid. *J. Fluid Mech.* **614**, 355–380.

Breder, C. M. 1926 The locomotion of fishes. *Zoologica* **4**, 159–291.

Butkov, E. 1968 *Mathematical physics*. Addison-Wesley, Reading.

Chang, X., Zhang, L. & He, X. 2012 Numerical study of the thunniform mode of fish swimming with different reynolds number and caudal fin shape. *Computers and Fluids* **68**, 54–70.

Dewey, P. A., Boschitsch, B. M., Moored, K. W., Stone, H. A. & Smits, A. J. 2013 Scaling laws for the thrust production of flexible pitching panels. *J. Fluid Mech.* **732**, 29–46.

Dong, G. J. & Lu, X. Y. 2007 Characteristics of flow over traveling wavy foils in a side-by-side arrangement. *Phys. Fluids* **19**, 057107.

Eloy, C. 2013 On the best design for undulatory swimming. *J. Fluid Mech.* **717**, 48–89.

Eloy, C. & Schouveiler, L. 2011 Optimisation of two-dimensional undulatory swimming at high reynolds number. *Int. J. Non-Linear Mech.* **46**, 568–576.

Fernandez-Feria, R. 2016 Linearized propulsion theory of flapping airfoils revisited. *Phys. Rev. Fluids* **1**, 084502.

Fernandez-Feria, R. 2017 Note on optimum propulsion of heaving and pitching airfoils from linear potential theory. *J. Fluid Mech.* **826**, 781–796.

Fernandez-Feria, R. & Alaminos-Quesada, J. 2018 Unsteady thrust, lift and moment of a two-dimensional flapping thin airfoil in the presence of leading-edge vortices: a first approximation from linear potential theory. *J. Fluid Mech.* **851**, 344–373.

Floryan, D. & Rowley, C. W. 2018 Clarifying the relationship between efficiency and resonance for flexible inertial swimmers. *J. Fluid Mech.* **853**, 271–300.

Garrick, I. E. 1936 Propulsion of a flapping and oscillating airfoil. *Tech. Rep.* TR 567. NACA.

Heathcote, S. & Gursul, I. 2007 Flexible flapping airfoil propulsion at low Reynolds numbers. *AIAA J.* **45**, 1066–1079.

Hoover, A. P., Cortez, R., Tytell, E. D. & Fauci, L. J. 2018 Swimming performance, resonance and shape evolution in heaving flexible panels. *J. Fluid Mech.* **847**, 386–416.

Huera-Huarte, F. J. 2018 On the impulse produced by chordwise flexible pitching foils in a quiescent fluid. *J. Fluids Eng.* **140**, 041206.

Kang, C. K., Aono, H., Cesnik, C. E. S. & Shyy, W. 2011 Effects of flexibility on the aerodynamic performance of flapping wings. *J. Fluid Mech.* **689**, 32–74.

von Kármán, Th. & Sears, W. R. 1938 Airfoil theory for non-uniform motion. *J. Aeronaut. Sci.* **5**, 379–390.

Katz, J. & Weihs, D. 1978 Hydrodynamic propulsion by large amplitude oscillation of an aerofoil with chordwise flexibility. *J. Fluid Mech.* **88**, 485–497.

Le, T. Q., Ko, J. H., Byun, D., Park, S. H. & Park, H. C. 2010 Effect of chord flexure on aerodynamic performance of a flapping wing. *J. Bionic Eng.* **7**, 87–94.

Lighthill, M. J. 1969 Hydromechanics of aquatic animal propulsion. *Ann. Rev. Fluid Mech.* **1**, 413–449.

Lighthill, M. J. 1970 Aquatic animal propulsion of high hydromechanical efficiency. *J. Fluid Mech.* **44**, 265–301.

Lighthill, M. J. 1975 *Mathematical biofluiddynamics*. SIAM, Philadelphia.

Michelin, S. & Llewellyn Smith, S. G. 2009 Resonance and propulsion performance of a heaving flexible wing. *Phys. Fluids* **21**, 071902.

Moore, M. N. J. 2014 Analytical results on the role of flexibility in flapping propulsion. *J. Fluid Mech.* **757**, 599–612.

Moore, M. N. J. 2015 Torsional spring is the optimal flexibility arrangement for thrust production of a flapping wing. *Phys. Fluids* **27**, 091701.

Moore, M. N. J. 2017 A fast Chebyshev method for simulating flexible-wing propulsion. *J. Comput. Phys.* **345**, 792–817.

Newman, J. N. 1977 *Marine hydrodynamics*. The MIT Press, Cambridge (MA).

Olver, F. W. J. & Maximon, L. C. 2010 Bessel functions. In *NIST handbook of mathematical functions* (ed. F. W. J. Olver, D. W. Lozier, R. F. Boisvert & C. W. Clark), pp. 215–286. National Institute of Standards and Technology, Washington.

Paraz, F., Schouvelier, L. & Eloy, C. 2016 Thrust generation by a heaving foil: Resonance, nonlinearities, and optimality. *Phys. Fluids* **28**, 011903.

Pederzani, J. & Haj-Hariri, H. 2006 Analysis of heaving flexible airfoilsin viscous flow. *AIAA J.* **44**, 2773–2779.

Platzer, M., Jones, K., Young, J. & Lai, J. 2008 Flapping wing aerodynamics: progress and challenges. *AIAA J.* **46**, 2136–2149.

Polyanin, A. D. & Manzhirov, A. V. 1998 *Handbook of integral equations*. CRC Press, Boca Raton.

Prempraneerach, P., Hoover, F. S. & Triantafyllou, M. S. 2003 The effect of chordwise flexibility on the thrust and efficiency of a flapping foil. In *Proceedings of the Thirteenth International Symposium on Unmanned Untethered Submersible Technology*.

Ramananarivo, S., Godoy-Diana, R. & Thiria, B. 2011 Rather than resonance, flapping wings flyers may play on aerodynamics to improve performance. *Proc. Nat. Acad. Sci. USA* **108**, 5964–5969.

Shyy, W., Aono, H., Chimakurthi, S. K., Trizila, P., Kang, C. K., Cesnik, C. E. S. & Liu, H. 2010 Recent progress in flapping wing aerodynamics and aeroelasticity. *Prog. Aero. Sci.* **46**, 284–327.

Shyy, W., Aono, H., Kang, C. K. & Liu, H. 2013 *An Introduction to Flapping Wing Aerodynamics*. Cambridge University Press, Cambridge.

Theodorsen, T. 1935 General theory of aerodynamic instability and the mechanism of flutter. *Tech. Rep.* TR 496. NACA.

Tytell, E. D. 2004 The hydrodynamics of eel swimming: I. Wake structure. *J. of Exp. Biol.* **207**, 1825–1841.

Tzezana, G. A. & Breuer, K. S. 2019 Thrust, drag and wake structure in flapping compliant membrane wings. *J. Fluid Mech.* **862**, 871–888.

Vogel, S. 1994 *Life in moving fluids: The physical biology of flow*. Princeton University Press, Princeton.

Wang, S. & Zhang, L. J. 2016 Self-propulsion of flapping bodies in viscous fluids: Recent advances and perspectives. *Acta Mech. Sin.* **32**, 980–990.

Wu, J. C. 1981 Theory for the aerodynamic force and moment in viscous flows. *AIAA J.* **19**, 432–441.

Wu, T. Y. 1961 Swimming of a waving plate. *J. Fluid Mech.* **10**, 321–344.

Wu, T. Y. 1971*a* Hydromechanics of swimming propulsion. Part 2. Some optimum shape problems. *J. Fluid Mech.* **46**, 521–544.

Wu, T. Y. 1971*b* Hydromechanics of swimming propulsion. Part 1. Swimming of a two-dimensional flexible plate at variable forward speeds in an inviscid fluid. *J. Fluid Mech.* **46**, 337–355.

Wu, T. Y. 2011 Fish swimming and bird/insect flight. *Ann. Rev. Fluid Mech.* **43**, 25– 58.

Wu, T. Y., Brokaw, C. J. & C., Brennen, ed. 1975 *Swimming and flying in Nature, vols. 1 and 2*. Plenum Press, New York.

Zhang, D., Pan, G., Chao, L. & Zhang, Y. 2018 Effects of Reynolds number and thickness on an undulatory self-propelled foil. *Phys. Fluids* **30**, 071902.

Zhang, L. J. & Eldredge, J. D. 2009 A viscous vortex particle method for deforming bodies with application to biolocomotion. *Int. J. Num. Meth. Fluids* **59**, 1299–1320.

Zhu, Q. 2007 Numerical simulation of a flapping foil with chodwise or spanwise flexibility. *AIAA J.* **45**, 2448–2457.